

Kalman-filter-based track fitting in non-uniform magnetic field with segment-wise helical track model

Bo Li^a, Keisuke Fujii^{b,*}, Yuanning Gao^a

^a*Department of Engineering Physics, Tsinghua University, Beijing, 100084, China*

^b*High Energy Accelerator Research Organization (KEK), Tsukuba, 305-0801, Japan*

Abstract

In the future International Linear Collider (ILC) experiment, high performance tracking is essential to its physics program including precision Higgs studies. One of major challenges for a detector such as the proposed International Large Detector (ILD) is to provide excellent momentum resolution in a magnetic field with small (but non-negligible) non-uniformity. The non-uniform magnetic field implies deviation from a helical track and hence requires the extension of a helical track model used for track fitting in a uniform magnetic field. In this paper, a segment-wise helical track model is introduced as such an extension. The segment-wise helical track model approximates the magnetic field between two nearby measurement sites to be uniform and steps between the two sites along a helix. The helix frame is then transformed according to the new magnetic field direction for the next step, so as to take into account the non-uniformity of the magnetic field. Details of the algorithm and mathematical aspects of the segment-wise helical track model in a Kalman-filter-based track fitting in the non-uniform magnetic field are elaborated. The new track model is implemented and successfully tested in the framework of the Kalman filter tracking software package, KalTest, which was originally developed for tracking in a uniform magnetic field.

Keywords:

track fitting, non-uniform magnetic field, Kalman filter, transformation

*Corresponding author.

Email address: keisuke.fujii@kek.jp (Keisuke Fujii)

1. Introduction

One of the primary goals of the next generation e^+e^- collider, such as the International Linear Collider (ILC), is to make precise measurements of the properties of the Higgs boson thereby uncovering the secret of the electroweak symmetry breaking. This physics goal imposes great challenges on ILC detectors. For a main tracking detector, for instance, the momentum resolution $\delta(1/p_T)$ is required to be $O(10^{-4})$ $(\text{GeV}/c)^{-1}$ or better. The International Large Detector (ILD), one of the two conceptual detector designs currently pursued for the ILC experiments, uses a Time Projection Chamber (TPC) as its main tracking detector[1]. For the ILD TPC, the above required momentum resolution translates into about 200 sampling points along a track with a transverse spatial resolution of 100 μm or better over its full drift length of 2.2 m in a magnetic field of 3.5 T. New TPC readout techniques, based on Micro Pattern Gaseous Detector (MPGD) technologies having small $\mathbf{E} \times \mathbf{B}$ effect, good two-hit resolution, and excellent spatial resolution, provide a promising solution to satisfy the rigorous demand of the ILC.

In order to fulfill the required performance, however, the hardware R&Ds have to be backed by software developments that match the environment of the linear collider TPC. A Kalman filter software package, KalTest, has been successfully used for tracking in full detector simulations for physics feasibility studies as well as for tracking in test beam data taken with a Large Prototype (LP) TPC[2]. For the LP test, where the effect of the non-uniform magnetic field on the particle trajectory is small¹, we could use a helical track model as used in the original KalTest. However, the future real LCTPC such as the ILD TPC must work in a non-uniform magnetic field with a non-uniformity up to a few percent[3]. In principle, Kalman filter algorithm itself is independent of the track model and can adapt to the non-uniform magnetic field. The most general solution is to implement a generic track model together with a Runge-Kutta track propagator. For the modest non-uniformity, this solution might not be optimal from the CPU time point of view. In this paper, another solution, a segment-wise helical

¹ There are two major ways for the presence of a non-uniform magnetic field to manifest itself: (1) $\mathbf{E} \times \mathbf{B}$ effect that distorts the measured hit points and hence the apparent trajectory and (2) the real deviation of a track from a helical trajectory. The former effect can be corrected away in principle. As long as the latter is negligible, we can therefore use the helical track model.

32 track model, is proposed. It will be shown that the implementation of the
 33 segment-wise helical track model that replaces the original simple helical
 34 track model allows us to successfully realize Kalman-filter-based track fitting
 35 in a moderate non-uniform magnetic field with the minimal change to the
 36 original KalTest package. The time consumption of track fitting in the non-
 37 uniform magnetic field will also be discussed.

38 2. KalTest

39 KalTest is a ROOT[4] based Kalman filter software package written in
 40 C++ for track fitting in high energy physics experiments. Comparing with
 41 the least square fitting method, the Kalman filter has great advantages in
 42 track fitting[5]. The basic formulae and their implementation in KalTest are
 43 summarized in this section, while details can be found in KalTest manual[6].

44 2.1. Kalman filter

45 The Kalman filter handles a system that evolves according to an equation
 46 of motion (*system equation*) under the influence of random disturbance (*pro-*
 47 *cess noise*). It is designed to provide the optimal estimate of the system's
 48 state at a given point from the information collected at multiple observation
 49 points (*measurement sites*). Suppose that there are n measurement sites
 50 ($k = 1, \dots, n$) and the state of the system at site (k) can be specified by a
 51 p -dimensional column vector (*state vector*) $\bar{\mathbf{a}}_k$, where the bar indicates that
 52 it is the true state vector without any measurement error. The system equa-
 53 tion that describes the evolution of the state at site ($k - 1$) to the next one,
 54 site (k), can be written in the form:

$$\bar{\mathbf{a}}_k = \mathbf{f}_{k-1}(\bar{\mathbf{a}}_{k-1}) + \mathbf{w}_{k-1}, \quad (1)$$

55 where $\mathbf{f}_{k-1}(\bar{\mathbf{a}}_{k-1})$ is a *state propagator* which expresses a smooth and deter-
 56 ministic motion that would take place if there were no process noise, and
 57 \mathbf{w}_{k-1} is the *process noise* term due to the random disturbance. It is assumed
 58 that the process noise is unbiased and has a covariance given by

$$\mathbf{Q}_{k-1} \equiv \langle \mathbf{w}_{k-1} \mathbf{w}_{k-1}^T \rangle. \quad (2)$$

59 At each site, we measure some observables about the system. The values
 60 of these observables comprise a m -dimensional column vector (*measurement*

61 vector) \mathbf{m}_k . Its relation to the state vector $\bar{\mathbf{a}}_k$ at site (k) is called a *measure-*
 62 *ment equation*:

$$\mathbf{m}_k = \mathbf{h}_k(\bar{\mathbf{a}}_k) + \boldsymbol{\epsilon}_k, \quad (3)$$

63 in which $\mathbf{h}_k(\bar{\mathbf{a}}_k)$ is a *projector* which gives, as a function of the state vector,
 64 the measurement vector you would expect for an ideal measurement with no
 65 measurement error, and $\boldsymbol{\epsilon}_k$ is the random measurement error (*measurement*
 66 *noise*) unavoidable in practice. We assume here that systematic errors such
 67 as those from misalignment of detectors have been corrected and hence the
 68 random measurement noise is unbiased and having a covariance given by

$$\mathbf{V}_k \equiv (\mathbf{G}_k)^{-1} \equiv \langle \boldsymbol{\epsilon}_k \boldsymbol{\epsilon}_k^T \rangle. \quad (4)$$

69 In the Kalman filter process, two operations, *prediction* and *filtering*, are
 70 needed at each site to proceed. The state vector prediction is the extrapola-
 71 tion of \mathbf{a}_{k-1}^{k-1} to the next site by using Eq.(1):

$$\mathbf{a}_k^{k-1} = \mathbf{f}_{k-1}(\mathbf{a}_{k-1}^{k-1}) \equiv \mathbf{f}_{k-1}(\mathbf{a}_{k-1}), \quad (5)$$

72 where the superscripts ($k-1$) to the state vectors indicate that the state
 73 vectors are estimated using the information up to site ($k-1$). In what
 74 follows we will omit the superscript, if the superscript coincides with the
 75 subscript as $\mathbf{a}_{k-1} \equiv \mathbf{a}_{k-1}^{k-1}$.

76 The covariance matrix for \mathbf{a}_{k-1} is defined by

$$\mathbf{C}_{k-1} \equiv \left\langle (\mathbf{a}_{k-1} - \bar{\mathbf{a}}_{k-1})(\mathbf{a}_{k-1} - \bar{\mathbf{a}}_{k-1})^T \right\rangle, \quad (6)$$

77 then the prediction for the covariance matrix at site (k) is given by

$$\mathbf{C}_k^{k-1} = \mathbf{F}_{k-1} \mathbf{C}_{k-1} \mathbf{F}_{k-1}^T + \mathbf{Q}_{k-1}, \quad (7)$$

78 where

$$\mathbf{F}_{k-1} \equiv \frac{\partial \mathbf{f}_{k-1}}{\partial \mathbf{a}_{k-1}} \quad (8)$$

79 is called a *propagation matrix*.

80 In the filtering step, the predicted state vector at site (k) is updated by
 81 taking into account the pull that is defined to be the difference between the
 82 measured and the predicted measurement vectors, $\mathbf{m}_k - \mathbf{h}_k(\mathbf{a}_k^{k-1})$, as

$$\mathbf{a}_k = \mathbf{a}_k^{k-1} + \mathbf{K}_k (\mathbf{m}_k - \mathbf{h}_k(\mathbf{a}_k^{k-1})), \quad (9)$$

83 in which, \mathbf{K}_k is the gain matrix given by

$$\mathbf{K}_k = \left[(\mathbf{C}_k^{k-1})^{-1} + \mathbf{H}_k^T \mathbf{G}_k \mathbf{H}_k \right]^{-1} \mathbf{H}_k^T \mathbf{G}_k \quad (10)$$

84 with \mathbf{H}_k defined by

$$\mathbf{H}_k \equiv \frac{\partial \mathbf{h}_k}{\partial \mathbf{a}_k^{k-1}}, \quad (11)$$

85 which is called the *measurement matrix*.

86 After all the n sites are filtered, the state vector at site ($k(k < n)$) can
 87 be reevaluated by including the information at subsequent sites: $k + 1$ to n .
 88 This process is called *Smoothing*. The smoothed state at site (k) is obtained
 89 by the following backward recurrence formula

$$\begin{cases} \mathbf{a}_k^n &= \mathbf{a}_k + \mathbf{A}_k (\mathbf{a}_{k+1}^n - \mathbf{a}_{k+1}^k) \\ \mathbf{A}_k &= \mathbf{C}_k \mathbf{F}_k^T (\mathbf{C}_{k+1}^k)^{-1} \end{cases}, \quad (12)$$

90 which gives the smoothed state at site (k) in terms of the smoothed state at
 91 site ($k + 1$), the predicted state at site ($k + 1$), and the filtered state at site
 92 (k).

93 2.2. Helical track parametrization

94 In a uniform magnetic field a charged particle follows a helical trajectory.
 95 If we set our coordinate system in such a way that the magnetic field points
 96 to the z axis direction, the helix can be parametrized as

$$\begin{cases} x &= x_0 + d_\rho \cos \phi_0 + \frac{\alpha}{\kappa} (\cos \phi_0 - \cos(\phi_0 + \phi)) \\ y &= y_0 + d_\rho \sin \phi_0 + \frac{\alpha}{\kappa} (\sin \phi_0 - \sin(\phi_0 + \phi)) \\ z &= z_0 + d_z - \frac{\alpha}{\kappa} \tan \lambda \cdot \phi \end{cases}, \quad (13)$$

97 where $\mathbf{x}_0 = (x_0, y_0, z_0)$ is an arbitrary reference point on which three (d_ρ ,
 98 ϕ_0 , and d_z) out of the five helix parameters, d_ρ , ϕ_0 , κ , d_z , and $\tan \lambda$, depend
 99 and α is a constant defined by $\alpha \equiv 1/cB$ with B and c being the magnetic
 100 field and the speed of light, respectively. Since the reference point \mathbf{x}_0 is
 101 arbitrary, we can take it to be the measured hit point at each site, say, site
 102 (k) and call it a pivot. Then ϕ measures the deflection angle from the pivot.
 103 The geometrical meanings of the five helix parameters are depicted in Fig.1.
 104 Notice that $\rho \equiv \alpha/\kappa$ is the radius of the helix singled by the particle charge,
 105 while $\kappa \equiv Q/p_t$ with Q being the charge in units of the elementary charge

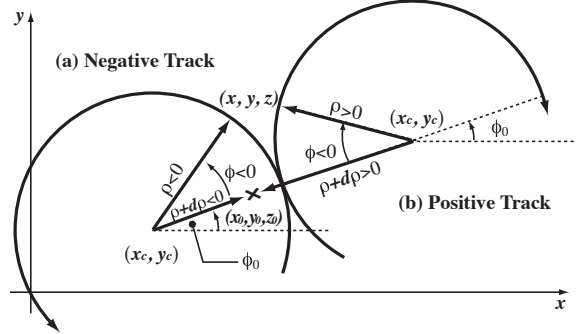


Figure 1: Helical track parametrization in KalTest. $\mathbf{x} = (x, y, z)$ is a point on the helix, $\mathbf{x}_0 = (x_0, y_0, z_0)$ a reference point usually taken to be a hit point. d_ρ is the distance of the helix from the pivot in the x - y plane, ϕ_0 the azimuthal angle of the pivot with respect to the center of the helix, d_z the distance of the helix from the pivot in the z direction, and λ stands for the dip angle.

106 and p_t being the transverse momentum. The five parameters in Eq.(13) are
 107 combined to make a concrete state vector

$$\mathbf{a}_k = (d_\rho, \phi_0, \kappa, d_z, \tan \lambda)^T .$$

108 The reason to use $\kappa = Q/p_t$ instead of ρ or p_t as a helix parameter is to
 109 allow continuous change of the state vector for a high momentum track for
 110 which the curvature might change its sign during the track fitting. Notice
 111 that there is a difference of π in the definition of ϕ_0 , depending on the track
 112 charge. This is to avoid discontinuity of ϕ_0 that would happen if κ changes
 113 its sign during track fitting.

114 2.3. Implementation

115 Notice that the formalism presented above is generic, though the concrete
 116 forms of the state propagator $\mathbf{f}_{k-1}(\mathbf{a}_{k-1})$, the projector $\mathbf{h}_k(\mathbf{a}_k^{k-1})$, and their
 117 derivatives, \mathbf{F}_{k-1} and \mathbf{H}_k , depend on the track model and the geometry and
 118 distribution of the measurement sites. In order to keep the application scope
 119 of this generic formalism as wide as possible, KalTest is designed to extract
 120 this generic part as a separate sub-package (KalLib) that forms an abstract
 121 layer consisting of abstract base classes that implement the generic Kalman
 122 filter algorithm. In order to realize Kalman-filter-based track fitting, we then
 123 inherit from the generic base classes in the abstract base class library KalLib

124 and implement their pure virtual methods for track fitting in a tracking de-
 125 tector consisting of measurement layers. The resultant Kalman-filter-based
 126 track fitter library is KalTrackLib. KalTrackLib, however, should not de-
 127 pend on any particular track model or shape or coordinate system of any
 128 measurement layer so as to accommodate variety of tracking devices which
 129 may coexist in the same tracking system. KalTrackLib is hence designed
 130 to interact with concrete track model or concrete measurement layer classes
 131 always through interface classes that represent an abstract track or an ab-
 132 stract measurement layer class. The implementation of concrete track models
 133 (helix, straight line, etc.) and measurement surfaces (cylinder, hyperbolic,
 134 flat plane, conical surface, etc.) are separated out into a geometry library
 135 eomLib.

136 Figure 2 shows some major classes contained in these three packages. In
 137 the KalLib library, TVKalSystem is implemented as an array of TVKalSite-
 138 derived objects and represents a collection of information gathered at each
 139 measurement site. Each TVKalSite-derived object can contain up to three
 140 Kalman filter states (i.e. predicted, filtered, and smoothed), each of them
 141 being an instance of some concrete class inheriting from TVKalState. The
 142 functions TVKalState::Propagate() and TVKalSite::Filter() implement
 143 Eqs.(7) and (9), respectively. The pure virtual functions such as TVKalState::MoveTo(),
 144 TVKalSite::CalcExpectedMeasVec(), and TVKalSite::CalcMeasVecDerivative()
 145 declared in the two classes are implemented in the corresponding derived
 146 classes of KalTrackLib. These concrete functions in the derived classes in-
 147 teract with a track model or a measurement layer through the abstract layer
 148 made of TVTrack, TVSurface, and TVMeasLayer and are still quite generic.
 149 The concrete geometrical features of the track or the measurement layers are
 150 supplied by concrete classes in GeomLib, where, for instance, the helical track
 151 model defined by Eq.(13) is implemented in a class called THelicalTrack de-
 152 rived from TVTrack, which actually propagates and calculates the concrete
 153 value of the state vector \mathbf{a} , the propagation matrix \mathbf{F} , and the covariance
 154 matrix \mathbf{C} and a cylindrical surface is implemented in a class called TCylinder
 155 inheriting from TVSurface.

156 The architectural design of KalTest thus minimizes the number of user-
 157 implemented classes to the following three:

- 158 • **MeasLayer**: a measurement layer object that multiply inherits from a
 159 concrete shape class such as TCylinder and the abstract measurement
 160 layer class TVMeasLayer.

- 161 • **KalDetector**: a class derived from `TVKalDetector`, which is imple-
162 mented as an array of `TVMeasLayer` pointers and holds `MeasLayers`
163 with any shape and coordinate system as well as materials.
- 164 • **Hit**: a coordinate vector class as defined by the `MeasLayer` class, which
165 inherits from `TVTrackHit`.

Notice that, by design, `KalTest` allows site-to-site change of track models.

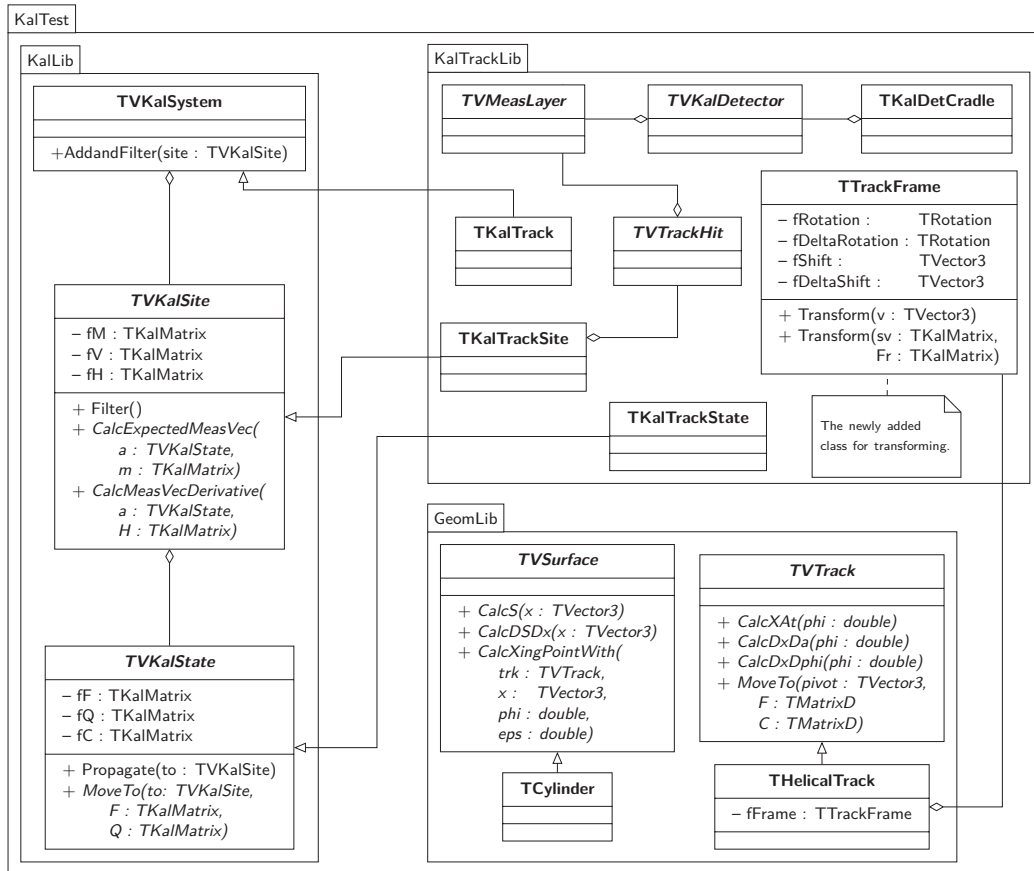


Figure 2: Class diagram of `KalTest`. `KalLib` contains the generic Kalman filter procedure. The pure virtual functions specific to tracking are implemented in `KalTrackLib`. Basic geometrical objects to express detector configuration or to represent track models are implemented in `GeomLib`.

166 Since the original helical track model in `KalTest` is valid only in a uniform
167 magnetic field, the result of track fitting will not be satisfactory if the track
168

169 is generated in a significantly non-uniform magnetic field, as we will see in
 170 Sec.4. A new class in the KalTrackLib library, `TTrackFrame`, which contains
 171 the algorithm for transforming a coordinate frame in a non-uniform magnetic
 172 field, can solve this issue and will be described in the next section.

173 3. Algorithm for non-uniform magnetic field

174 3.1. Basic idea

175 If the non-uniformity of the magnetic field is not too large, we can assume
 176 that the magnetic field between two measurement layers is approximately
 177 uniform. We can then propagate our track from one measurement layer to the
 178 next using the helix model we discussed above. When the track reaches the
 179 next layer, we update the magnetic field in order to take the non-uniformity
 180 into account, and propagate the track with the updated magnetic field. The
 181 track produced this way is hence segment-wise helical and hereafter called a
 182 *segment-wise helical track*. Notice that the direction of the magnetic field also
 183 changes as well as its magnitude in general. We therefore need to attach, to
 184 each track segment, a local frame having its z axis pointing to the magnetic
 185 field direction so as to use our helix parametrization defined in Eq.(13). At
 186 the end of each step, we hence update the frame to make its z axis parallel
 187 with the magnetic field there and transform the propagated state vector to
 188 this new updated frame.

This new track propagation procedure is illustrated in Fig.3. Firstly, the

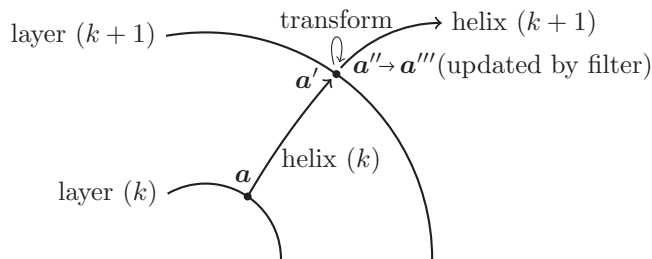


Figure 3: Basic idea of transforming the state vector and the associated frame between two nearby layers.

189 state vector $\mathbf{a} = \mathbf{a}_k$ at layer (k) is propagated to \mathbf{a}' at layer ($k + 1$) along
 190 helix (k) parametrized by Eq.(13). The magnetic field at the intersection
 191 of the helix and layer ($k + 1$) is then calculated. With the new magnetic
 192 field, the state vector is updated to \mathbf{a}''' .

193 field and the one at the last intersection, the matrix for rotating the frame
 194 can be obtained. Since the state vector is not easy to transform directly, it
 195 is converted to the momentum vector. Applying the rotation matrix to the
 196 momentum vector and then using the rotated momentum, we can calculate
 197 the predicted state vector \mathbf{a}'' in the new frame. Notice that this defines a new
 198 modified state propagator as $\mathbf{a}'' \equiv \mathbf{a}_{k+1}^k = \mathbf{f}_k^{\text{mod}}(\mathbf{a}_k)$. Finally, we update the
 199 predicted state vector in the new frame with Eq.(9), getting the filtered state
 200 vector $\mathbf{a}''' \equiv \mathbf{a}_{k+1}$. The same procedure is repeated for subsequent steps.

201 Since the propagation procedure or equivalently the propagator function
 202 is modified, the propagator matrix should also be modified accordingly. We
 203 will explain how in the next subsection.

204 3.2. Transformation

205 The transformation between the two frames consists of a shift and a
 206 rotation as is illustrated in Fig.4. The shift is given by the vector $\Delta \mathbf{d}_k$ and
 207 parallel-transport the xyz -frame at the starting point on layer (k) to the
 208 new $x'y'z'$ -frame at the predicted intersection on layer ($k+1$). The $x'y'z'$ -
 209 frame is then rotated so as to make the z'' axis point to the new magnetic
 210 field. This rotation $\Delta \mathbf{R}$ is defined as follows:

$$\Delta \mathbf{R} = \Delta \mathbf{R}_{z''}(-\phi) \Delta \mathbf{R}_{y''}(\theta) \Delta \mathbf{R}_{z'}(\phi), \quad (14)$$

211 where the $x'y'z'$ -frame is first rotated around the z' axis by the angle ϕ to
 212 bring the y' axis to a tentative y'' axis so that it becomes perpendicular to
 213 the plane spanned by the z' axis and the new magnetic field direction; the
 214 frame is then rotated by the angle θ around the tentative y'' axis to make the
 215 z'' axis point to the new magnetic field direction; finally the frame is rotated
 216 again this time around the z'' axis by the angle $-\phi$ to bring the tentative y''
 217 axis to its final direction.

218 Since the rotation is passive for a vector, the rotation matrices are given
 219 by

$$\Delta \mathbf{R}_{z'}(\phi) = \begin{pmatrix} \cos \phi & \sin \phi & 0 \\ -\sin \phi & \cos \phi & 0 \\ 0 & 0 & 1 \end{pmatrix}$$

220 and

$$\Delta \mathbf{R}_{y''}(\theta) = \begin{pmatrix} \cos \theta & 0 & -\sin \theta \\ 0 & 1 & 0 \\ \sin \theta & 0 & \cos \theta \end{pmatrix}.$$

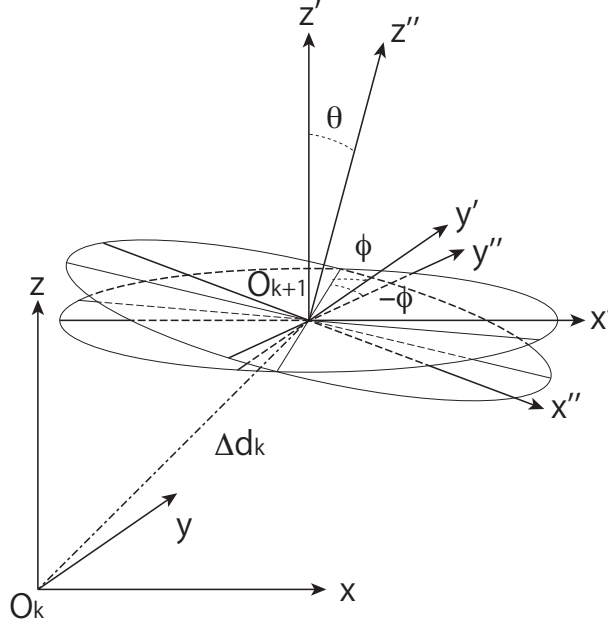


Figure 4: Transformation from one frame to the next. The θ and ϕ angles are determined by the magnetic field directions at the position \mathbf{O}_k and \mathbf{O}_{k+1} .

221 Considering the shift and the rotation, a local position vector \mathbf{x}_k in frame
 222 (k) can be transformed to a local position vector in frame ($k + 1$) by

$$\mathbf{x}_{k+1} = \Delta \mathbf{R}_k (\mathbf{x}_k - \Delta \mathbf{d}_k). \quad (15)$$

223 We also need a transformation of a vector from a global frame to the local
 224 frame:

$$\mathbf{x}_{k+1} = \mathbf{R}_k (\tilde{\mathbf{x}} - \mathbf{d}_k), \quad (16)$$

225 in which $\tilde{\mathbf{x}}$ is the corresponding vector defined in the global frame. In Eq.(15),
 226 \mathbf{x}_k is defined in local frame (k), and it can be transformed from the global
 227 vector by

$$\mathbf{x}_k = \mathbf{R}_{k-1} (\tilde{\mathbf{x}} - \mathbf{d}_{k-1}) \quad (17)$$

228 Substituting Eq.(17) into Eq.(15)

$$\mathbf{x}_{k+1} = \Delta \mathbf{R}_k [\mathbf{R}_{k-1} (\tilde{\mathbf{x}} - \mathbf{d}_{k-1}) - \Delta \mathbf{d}_k],$$

229 then the global rotation matrix \mathbf{R}_k and the shift vector \mathbf{d}_k can be represented

230 by the following recurrence formulae:

$$\begin{cases} \mathbf{R}_k &= \Delta \mathbf{R}_k \mathbf{R}_{k-1} \\ \mathbf{d}_k &= \mathbf{d}_{k-1} + \mathbf{R}_{k-1}^{-1} \Delta \mathbf{d}_k \end{cases} . \quad (18)$$

231 The local magnetic field in frame (k) is transformed simply by

$$\mathbf{B}(\mathbf{x}) = \mathbf{R}_k \tilde{\mathbf{B}}(\tilde{\mathbf{x}}), \quad (19)$$

232 in which $\tilde{\mathbf{B}}(\tilde{\mathbf{x}})$ is the magnetic field in the global frame.

233 3.3. Propagator matrix

234 The total propagation described in Section 3.1 can be represented math-
235 ematically by

$$\begin{cases} \mathbf{a}' &= \mathbf{f}_k(\mathbf{a}_k) \\ \mathbf{p} &= \mathbf{c}(\mathbf{a}') \\ \mathbf{p}' &= \mathbf{t}(\mathbf{p}) \\ \mathbf{a}'' &= \mathbf{c}^{-1}(\mathbf{p}') \end{cases} , \quad (20)$$

236 where, the function \mathbf{f}_k is the original state vector propagation function for a
237 uniform magnetic field, \mathbf{c} is a function which converts a state vector to the
238 corresponding momentum with \mathbf{c}^{-1} being its inverse, and the function \mathbf{t} is a
239 rotation given by the rotation matrix $\Delta \mathbf{R}$.

240 The momentum can be calculated using Eq.(13):

$$\mathbf{p} = - \left(\frac{Q}{\alpha} \right) \frac{d\mathbf{x}}{d\phi} = \frac{1}{|\kappa|} \begin{pmatrix} -\sin \phi_0 \\ \cos \phi_0 \\ \tan \lambda \end{pmatrix} . \quad (21)$$

241 As mentioned before, the sign of κ is the sign of the particle charge. The
242 momentum vectors in the two successive local frames are related by $\Delta \mathbf{R}$:

$$\mathbf{p}' = \Delta \mathbf{R} \mathbf{p}. \quad (22)$$

243 During the transformation, the intersection (taken to be the pivot) is on the
244 helix. Therefore the two distance components, d_ρ and d_z , are zero, while
245 the other three components, ϕ_0 , κ , and $\tan \lambda$, can easily be solved from the
246 momentum by their definitions:

$$\mathbf{a}'' = \begin{pmatrix} d_\rho \\ \text{atan2}(-p'_x, p'_y) \\ \frac{s_\kappa}{(p_x'^2 + p_y'^2)^{\frac{1}{2}}} \\ d_z \\ \frac{p'_z}{(p_x'^2 + p_y'^2)^{\frac{1}{2}}} \end{pmatrix} , \quad (23)$$

247 where the sign of κ in the last local frame (i.e. $s_\kappa \equiv \text{sgn}(\kappa)$) is used, since
 248 it is safe to assume that the magnetic field direction will not be reversed as
 249 long as the magnetic field varies moderately.

250 According to Eq.(20), the modified propagator matrix is given by

$$\mathbf{F}_k^{\text{mod}} \equiv \frac{\partial \mathbf{f}_k^{\text{mod}}(\mathbf{a})}{\partial \mathbf{a}} = \frac{\partial \mathbf{a}''}{\partial \mathbf{a}}, \quad (24)$$

251 which is calculated to be

$$\mathbf{F}_k^{\text{mod}} = \frac{\partial \mathbf{a}''}{\partial \mathbf{p}'} \frac{\partial \mathbf{p}'}{\partial \mathbf{p}} \frac{\partial \mathbf{p}}{\partial \mathbf{a}'} \frac{\partial \mathbf{a}'}{\partial \mathbf{a}} = \mathbf{F}_k^{\text{rot}} \mathbf{F}_k. \quad (25)$$

252 The original propagator matrix \mathbf{F}_k is known in the original KalTest already.
 253 The other three matrices in $\mathbf{F}_k^{\text{rot}}$ are given in Appendix A.

254 The transformation algorithm described in this section is implemented
 255 in the class `TTrackFrame`. In order to promote our `THelicalTrack` class to
 256 accommodate the segment-wise helical track model for non-uniform magnetic
 257 field, a `TTrackFrame` object is added as its data member. With the help
 258 of `TTrackFrame`, the `THelicalTrack` can calculate the global position, the
 259 modified state vector, and the modified propagator matrix. This way, all the
 260 modifications for the segment-wise helical track implementation are hidden in
 261 `THelicalTrack` and are invisible to the other classes. Because of the locality
 262 of the segment-wise helical track model implementation, it can be seen that
 263 the track smoothing is still valid from Eq.(12). Further it should be relatively
 264 easily ported into any Kalman filter package other than KalTest.

265 4. Test of algorithm

266 4.1. Simulation conditions

267 After the algorithm for track fitting in a non-uniform magnetic field was
 268 implemented based on the original KalTest code, its track reconstruction
 269 performance has been tested intensively. Firstly, the mean and the sigma
 270 of momentum distributions were compared for the original code and the
 271 new code. As expected, the results are identical if tracks are generated and
 272 reconstructed in a uniform magnetic field.

273 For the purpose of testing track reconstruction in a non-uniform magnetic
 274 field, we assumed the following (artificially non-uniform) magnetic field \mathbf{B} :

$$\begin{cases} B_x = B_0 kxz \\ B_y = B_0 kyz \\ B_z = B_0(1 - kz^2) \end{cases},$$

275 in which, $k = \frac{k_0}{z_{\max} r_{\max}}$, $B_0 = 3$ T, $z_{\max} = r_{\max} = 3000$ mm. The coefficient
 276 k can be set to several values for different non-uniformities. In simulation,
 277 we assumed a tracker having 251 measurement layers with a layer-to-layer
 278 distance of 6 mm, an inner radius of 300 mm, and outer radius of 1800 mm.
 279 The detector geometry is similar to the configuration of the LC TPC in the
 280 ILD detector concept[1].

281 To simulate tracks in the non-uniform magnetic field, a Runge-Kutta
 282 propagator class in ROOT[4], `TEveTrackPropagator`, was used. In this class,
 283 the position is a function of the length along the track and the crossing
 284 point of the track with a measurement layer is calculated by the bisection
 285 method. The crossing point was smeared to make a hit position according
 286 to the detector spatial resolution (100 μm) in the $r\phi$ plane. For the track
 287 generation, we generated dip angles and an azimuthal angles uniformly in
 288 $\lambda \in [0, 0.5]$ and $\phi \in [0, 2\pi]$, respectively. In Fig.5, a typical event display
 289 is shown for a track generated in the non-uniform magnetic field with $k_0 = 5$.
 290 In the same figure, for comparison, a track with the same initial momentum
 291 but in a uniform magnetic field ($k_0 = 0$) is also shown. Notice that the
 292 third component of \mathbf{B} depends on the z position quadratically in our field
 293 assumption, therefore the discrepancy of the two tracks increases as their z
 position becomes large.

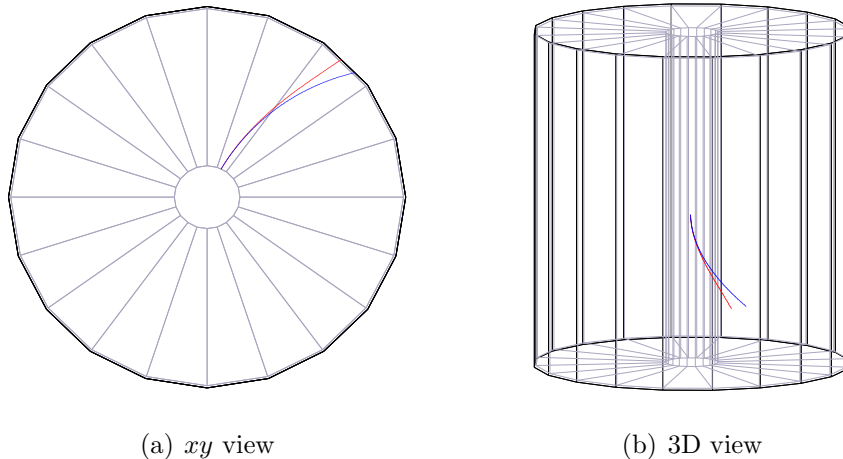


Figure 5: Event display. Tracks with 2 GeV/ c simulated in a non-uniform magnetic field (red curve: $k_0 = 5$) and uniform magnetic field (blue curve: $k_0 = 0$).

294 *4.2. Results*

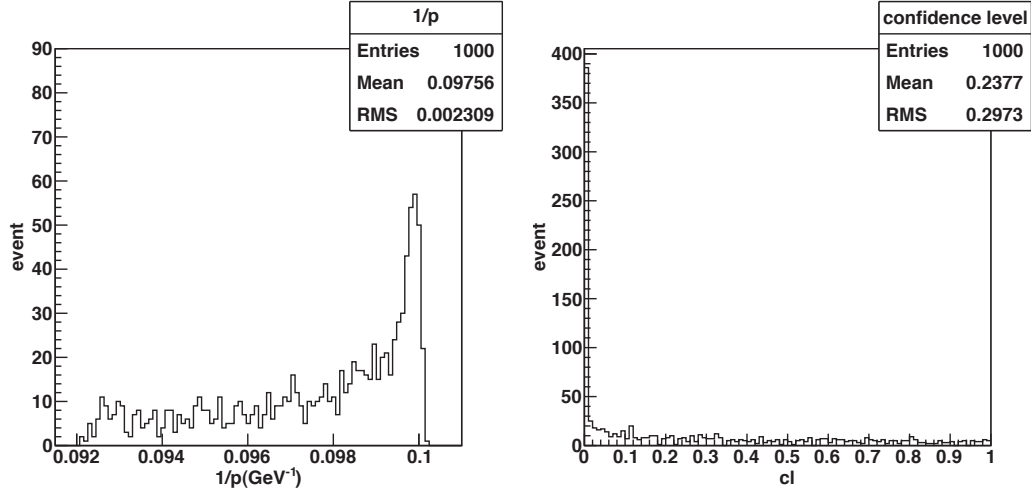
295 *4.2.1. Momentum measurement*

296 With tracks generated in the non-uniform magnetic field, we compared
297 the reconstructed reciprocal momentum and confidence level distributions for
298 the track-fit results using the original helical track model assuming a uniform
299 field and those using the segment-wise helical track model in Fig.6. The total
300 momentum is calculated as $p = p_t \sqrt{1 + \tan^2 \lambda}$, in which p_t and $\tan \lambda$ are the
301 fitted parameters in the state vector. In Fig.6(a), we used the original helical
302 track model with a uniform magnetic field: $\mathbf{B} = (0, 0, 3 \text{ T})$ to reconstruct
303 the tracks. The distribution of the reciprocal momentum on the left panel
304 of Fig.6(a) is non-gaussian, and the confidence level distribution on the right
305 panel has a delta-function-like peak at zero, indicating that the fitting is
306 inconsistent with the simulated tracks. This is exactly why the simple helical
307 track model used in the original KalTest must be updated for the non-uniform
308 magnetic field situation for future linear collider experiments.

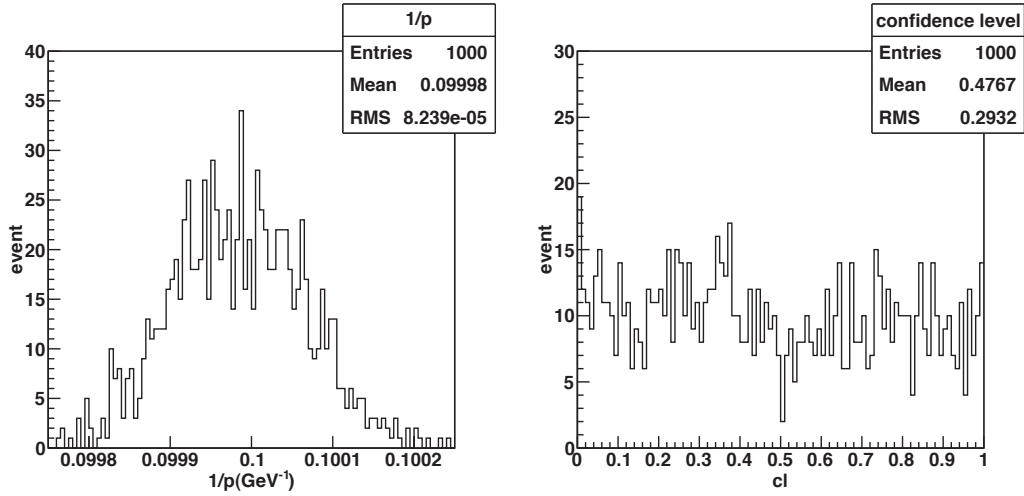
309 The result reconstructed with the segment-wise helical track model as-
310 suming the same magnetic field as that of the track generation is shown in
311 Fig.6(b). The mean value of the momentum distribution on the left panel
312 is very close to the expected, $0.1 (\text{GeV}/c)^{-1}$, and its standard deviation is
313 consistent with Gluckstern's formula[7]. The flat confidence level distribu-
314 tion on the right panel implies the fitted tracks and hits are also consistent.
315 Therefore, from Fig.6(a) and 6(b), it can be concluded that the improved al-
316 gorithm with the segment-wise helical track model performs much better in
317 track reconstruction since the non-uniformity of the magnetic field is properly
318 taken into account.

319 In fact, the bad resolution in Fig.6(a) was found to come from a momen-
320 tum bias. This is because the magnetic field becomes weaker as z increases,
321 although it is assumed to be constant in the reconstruction with the original
322 helical track model, thereby overestimating p_t . Since the magnetic field de-
323 creases with the z coordinate, as the dip angle increases, the reconstructed
324 $1/p_t$ decreases.

325 The results for different non-uniformities and dip angles with a track step
326 size (i.e. helix segment size) of 6 mm are given in Table 1(a). As expected,
327 for a specified dip angle, the momentum bias becomes more prominent as
328 the non-uniformity increases, since the assumption that the magnetic field
329 is approximately uniform between two nearby layers becomes inappropriate.



(a) Reconstructed in uniform magnetic field



(b) Reconstructed in non-uniform magnetic field

Figure 6: Comparison of track-fit results with the original helical track model and those with the segment-wise helical track model for tracks generated in a non-uniform magnetic field. The tracks were generated with the coefficient k_0 of the non-uniformity being 1, and the momentum 10 GeV/c.

Table 1: Mean and RMS of $1/p$ (in units of $10^{-1} \cdot (\text{GeV}/c)^{-1}$ and $10^{-5} \cdot (\text{GeV}/c)^{-1}$, respectively)

(a) Step size 6 mm			
k_0	$\lambda = 0.1$	$\lambda = 0.3$	$\lambda = 0.5$
0.5	1.0000/8.02	0.9999/7.79	0.9998/7.34
1	1.0000/8.03	0.9998/7.89	0.9995/7.65
2	1.0000/8.05	0.9997/8.09	0.9990/8.36
3	0.9999/8.07	0.9995/8.31	0.9984/9.20

(b) Step size 1 mm			
k_0	$\lambda = 0.1$	$\lambda = 0.3$	$\lambda = 0.5$
0.5	1.0000/8.02	1.0000/7.79	1.0000/7.34
1	1.0000/8.03	1.0000/7.89	0.9999/7.65
2	1.0000/8.05	0.9999/8.10	0.9998/8.36
3	1.0000/8.07	0.9999/8.32	0.9997/9.21

330 By the same token, the bias grows with the dip angle. Table 1(b) tells us that
 331 the mean value can be improved by adding dummy stepping layers to make
 332 the helix segment short enough and consequently the algorithm is forced to
 333 reevaluate the magnetic field at more stepping points. Tables 1(a) and 1(b)
 334 for the different step sizes have consistent momentum resolutions and as the
 335 non-uniformity becomes large the momentum resolution also increases be-
 336 cause the average magnetic field experienced by the tracks becomes smaller.
 337 This explanation is also valid for the dip angle dependence for a fixed k_0
 338 value (2 or 3). For the low non-uniformity values (0.5 or 1), the momentum
 339 resolution is dominated by the lever arm length and hence as λ increases, the
 340 transverse momentum gets smaller, and the resolution gets better.

341 4.2.2. CPU time

342 The time consumption of relevant functions in the track fitting (without
 343 the dummy layers to force the stepping size to be 1 mm) for 1000 tracks is
 344 listed in Table 2. These CPU times were measured on a laptop PC with a
 345 2.4 GHz Intel Core 2 Duo processor. The sum of CPU times consumed by
 346 track propagation and filtering turned out to essentially be the total track
 347 fitting time. From Table 2, one can see that the time consumption increased

Table 2: Time expense of relevant functions with the segment-wise helical track model for 1000 tracks in units of sec..

Function	Time expense
Total	18.82
TVKalState::Propagate	11.53
TVKalSite::Filter	7.27
TTrackFrame::TTrackFrame	0.87
TTrackFrame::TransformVector	6.59
TTrackFrame::TransformSv	2.58
TVSurface::CalcXingPointWith	5.90

348 by about 10 seconds because of using the track frame transformation class,
349 which was absent in the original KalTest. This means that the CPU ex-
350 pense was approximately doubled by the introduction of the segment-wise
351 helical track model. The functions transforming vectors are called many
352 times mostly in the function calculating the crossing points. One possibility
353 to reduce this time consumption is to optimize the number of calls for the
354 crossing point calculating function.

355 5. Summary

356 The helical track model in KalTest has been updated for the track fitting
357 in a moderately non-uniform magnetic field by introducing the concept of
358 segment-wise helical track model and implemented in the `THelicalTrack`
359 class. The segment-wise helical track model assumes that the magnetic field
360 is approximately uniform between two nearby measurement sites and ap-
361 proximates the track segment between the two sites to be a helix determined
362 by the track momentum and the magnetic field at the starting site of the
363 step. The non-uniformity of the magnetic field is then taken into account
364 by reevaluating the magnetic field at the end site of the step for the next
365 step. This requires the segment-wise helical track object `THelicalTrack` to
366 carry a coordinate frame object `TTrackFrame` as its data member to specify
367 the local coordinate system in which the state vector consisting of the he-
368 lix parameters is defined. The helix frame is then transformed at each step
369 so as to make the local z axis pointing to the new magnetic field direction.
370 The coordinate transformation modifies the original state propagator and its

371 derivative. In this paper we have elaborated the mathematical formulation
372 of the modifications for Kalman-filter-based tracking. It should be empha-
373 sized that the modifications are localized in the `THelicalTrack` class and
374 hence are invisible to the other part of the `KalTest` classes. This significantly
375 facilitated the implementation of the code to handle the non-uniform mag-
376 netic field since there was essentially no need to touch the original `KalTest`
377 architecture except for the track model `THelicalTrack` and its supporting
378 class `TTrackFrame`. The algorithm should hence be relatively easy to port to
379 any other Kalman-filter-based track fitting package.

380 We tested the segment-wise helical track model and its performance in
381 Kalman-filter-based track fitting in a non-uniform magnetic field. The test
382 showed that the track fitting with the segment-wise helical track model works
383 very well for a modest field non-uniformity and yields correct track momen-
384 tum values in the non-uniform magnetic field. It was also demonstrated
385 that the track fitting performance can be enhanced by adding dummy layers
386 (stepping layers) to reduce the step size so that the track fitting works in a
387 highly non-uniform field situation.

388 The CPU time expense was measured and found to be approximately
389 doubled as compared to the original `KalTest` for a uniform magnetic field.
390 The increase was mostly due to the repeated coordinate transformations for
391 various objects in stepping, calculations of crossing points of the track and
392 measurement layers in particular. It can probably be improved by optimizing
393 the code for the crossing point calculations.

394 The source code of the new `KalTest` with the segment-wise helical track
395 model can be downloaded from <http://www-jlc.kek.jp/jlc/en/subg/soft/tracking/kaltest->

396 **Acknowledgment**

397 The original `KalTest` package was developed in the frame work of the
398 LCTPC collaboration. We would like to thank all the developers including
399 K. Hoshina, Y. Nakashima, and A. Yamaguchi for their significant contribu-
400 tions in the early stage of the development. The authors are grateful to the
401 ILD software team and the members of the LCTPC group for useful discus-
402 sions and supports for this work. Among them Steve Aplin and Frank Gaede
403 deserve special mention. Their efforts to integrate the original `KalTest` pack-
404 age into the standard ILD event reconstruction chain and to test it throughly
405 in various simulation studies set a firm basis on which this work could be
406 built. The first author would like to thank the support from ILC group of

407 Institute of Particle and Nuclear Studies, KEK and LCD group of CERN.
 408 He also thanks to useful advice from Martin Killenberg. This work is sup-
 409 ported in part by the Creative Scientific Research Grant No. 18GS0202 of the
 410 Japan Society for Promotions of Science (JSPS), the JSPS Core University
 411 Program, and the JSPS Grant-in-Aid for Science Research No. 22244031,
 412 and the JSPS Specially Promoted Research No. 23000002. This work is also
 413 supported in part by National Natural Science Foundation of China under
 414 Contract Nos. 11075084, 11161140590.

415 Appendix A. The modified propagator matrix

416 The concrete form of $\mathbf{F}_k^{\text{rot}}$ in Eq.(25) is shown here. Notice first that
 417 at each step before the transformation to the new frame, the pivot of the
 418 predicted state vector is temporarily taken to be the predicted intersection
 419 of the track with the measurement layer there, implying that d_ρ and d_z
 420 are zero.² According to Eq.(21), the momentum calculation needs only the
 421 three non-zero parameters of the state vector. Now let the state vector
 422 $\mathbf{a}' = (\phi_0, \kappa, \tan \lambda)^T$, then the calculation of the first of the three derivatives
 423 in $\mathbf{F}_k^{\text{rot}}$ is straightforward:

$$\frac{\partial \mathbf{p}}{\partial \mathbf{a}'} = \begin{pmatrix} -\frac{1}{|\kappa|} \cos \phi_0 & \frac{s_\kappa}{\kappa^2} \sin \phi_0 & 0 \\ -\frac{1}{|\kappa|} \sin \phi_0 & -\frac{s_\kappa}{\kappa^2} \cos \phi_0 & 0 \\ 0 & -\frac{s_\kappa}{\kappa^2} \tan \lambda & \frac{1}{|\kappa|} \end{pmatrix}. \quad (\text{A.1})$$

424 According to Eq.(22), the second of the three derivatives in $\mathbf{F}_k^{\text{rot}}$ is

$$\frac{\partial \mathbf{p}'}{\partial \mathbf{p}} = \Delta \mathbf{R}. \quad (\text{A.2})$$

425 If we just use the non-zero components in Eq.(23), the derivative of the new
 426 state vector with respect to the momentum is

$$\frac{\partial \mathbf{a}''}{\partial \mathbf{p}'} = \begin{pmatrix} -\frac{p_y}{p_T^3} & \frac{p_x}{p_T^3} & 0 \\ -\frac{s_\kappa p_x}{p_T^3} & -\frac{s_\kappa p_y}{p_T^3} & 0 \\ -\frac{p_x p_z}{p_T^3} & -\frac{p_y p_z}{p_T^3} & \frac{1}{p_T^3} \end{pmatrix}. \quad (\text{A.3})$$

²After the frame transformation the pivot is moved to the actual hit position from the predicted intersection.

427 The product of the three matrices:

$$\mathbf{M} = \frac{\partial \mathbf{a}''}{\partial \mathbf{p}'} \frac{\partial \mathbf{p}'}{\partial \mathbf{p}} \frac{\partial \mathbf{p}}{\partial \mathbf{a}'}$$

428 is a 3×3 matrix. To use it in Eq.(25), the elements with zero values should
429 be restored, namely

$$\mathbf{F}_k^{\text{rot}} = \begin{pmatrix} 1 & 0 & 0 & 0 & 0 \\ 0 & M_{00} & M_{01} & 0 & M_{02} \\ 0 & M_{10} & M_{11} & 0 & M_{12} \\ 0 & 0 & 0 & 1 & 0 \\ 0 & M_{20} & M_{21} & 0 & M_{22} \end{pmatrix}. \quad (\text{A.4})$$

430 References

- 431 [1] T. Abe, et al., The International Large Detector: Letter of Intent,
432 arXiv:1006.3396.
- 433 [2] J. Abernathy, L. Bo, P. Conley, K. Dehmelt, R. Diener, et al., Recent
434 developments and status of MarlinTPC and related software, EUDET-
435 MEMO-2010-07.
- 436 [3] P. Schade, Correction methods for tpc operation in inhomogeneous mag-
437 netic fields, LC-DET-2010-001.
- 438 [4] I. Antcheva, M. Ballintijn, B. Bellenot, M. Biskup, R. Brun, et al.,
439 ROOT: A C++ framework for petabyte data storage, statistical anal-
440 ysis and visualization, Comput.Phys.Commun. 182 (2011) 1384–1385.
441 doi:10.1016/j.cpc.2011.02.008.
- 442 [5] R. Fruhwirth, Application of Kalman filtering to track and
443 vertex fitting, Nucl.Instrum.Meth. A262 (1987) 444–450.
444 doi:10.1016/0168-9002(87)90887-4.
- 445 [6] K. Fujii, Extended Kalman Filter, <http://www-jlc.kek.jp/subg/offl/kaltest>.
- 446 [7] R. Gluckstern, Uncertainties in track momentum and direction, due
447 to multiple scattering and measurement errors, Nucl.Instrum.Meth. 24
448 (1963) 381–389. doi:10.1016/0029-554X(63)90347-1.